Progress In Electromagnetics Research, Vol. 123, 447–465, 2012

FOURIER BASED COMBINED TECHNIQUES TO DESIGN NOVEL SUB-WAVELENGTH OPTICAL INTEGRATED DEVICES

L. Zavargo-Peche*, A. Ortega-Moñux, J. G. Wangüemert-Pérez, and Í. Molina-Fernández

Departamento Ingeniería de Comunicaciones, ETSI Telecomunicación, Universidad de Málaga, Málaga 29071, Spain

Abstract—We present a tool to aid the design of periodical structures, such as subwavelength grating (SWG) structures. It is based on the Fourier Eigenmode Expansion Method and includes the Floquet modes theory. Besides, the most interesting implemented functionalities to ease the design of photonic devices are detailed. The tool capabilities are shown using it to analyse and design three different SWG devices.

1. INTRODUCTION

According to the effective medium theory [1, 2], subwavelength gratings (SWG) are periodic structures that can implement homogeneous effective medium. This characteristic has been used to implement several structures, such us mirrors [3], fibre-to-chip grating couplers [4] or low loss and low crosstalk waveguide crossings [5], or high-pass filters [6].

The design of devices with periodic sections (e.g., SWG, photonic crystals [7], etc.) is usually performed using Finite Difference Time Domain (FDTD) simulations. However, analysis of periodic structures using FDTD is computationally very expensive, so a different approach is preferred in order to streamline the design of these nanophotonic periodic devices.

Eigenmode Expansion Methods (EEM), used together with Floquet mode theory [8–11] allows a significantly reduction in memory requirements and computational time when compared with FDTD. The first implementations of EEM used a classical Finite Difference

Received 29 July 2011, Accepted 19 October 2011, Scheduled 6 January 2012

* Corresponding author: Luis Zavargo-Peche (zavargo@ic.uma.es).

transversal discretization technique [8]. More recently, several implementations of the EEM based on the Fourier series expansion of the fields have been published [9–11]. These techniques are usually known as Fourier-EEM.

In this work, we have used a Fourier based Eigenmode Expansion Method which includes perfectly matched layer (PML) absorbing boundary conditions to deal with outgoing radiation and the Floquet formalism to efficiently analyse periodic devices. Using this highly efficient electromagnetic core, we have developed a CAD tool that facilitates the design of photonic structures with periodic sections. The utility of this tool has already been demonstrated with the successful design of a fibre-to-chip grating coupler for micrometric silicon rib waveguides [12, 13].

The main objective of this work is to show that the proposed tool is also a valuable resource for the design of state-of-the-art nanophotonic SWG devices, such as the multimode interference (MMI) coupler with subwavelength structures recently published in [14]. This paper is organized as follows. In Section 2, fundamentals of SWG structures are briefly described. Special attention will be paid later to explain the basics of the numerical method (Section 3), and the capabilities of the CAD tool (Section 4), which includes a complete set of design features (e.g., multiport definition, scattering matrix analysis, field and power monitors, optimization of physical and geometrical parameters, etc.). Finally, in Section 5 three different SWG devices (a directional coupler with SWG parallel waveguides and two MMI couplers with SWG claddings) have been designed. These examples show not only the capabilities of the proposed tool, but also the huge computational advantage of using Fourier- Eigenmode Expansion Methods when compared with FDTD techniques.

2. SUB-WAVELENGTH GRATINGS

A SWG is a periodic structure with a period short enough to suppress diffraction effects. When properly engineered, SWG structures can behave as homogeneous media, whose refractive index can be tuned by adjusting the SWG geometry [1], thereby allowing for completely new design approaches [15].

The SWG concept is shown in Figure 1(a), where a stratified medium composed of alternate layers with refractive indexes n_1 and n_2 is considered. Note that the medium extends infinitely in the X and Y directions. If the period length Λ is shorter than the shortest Bragg period, the stratified structure behaves as a homogeneous medium [1]. Note that, even when the constituent materials are isotropic, the

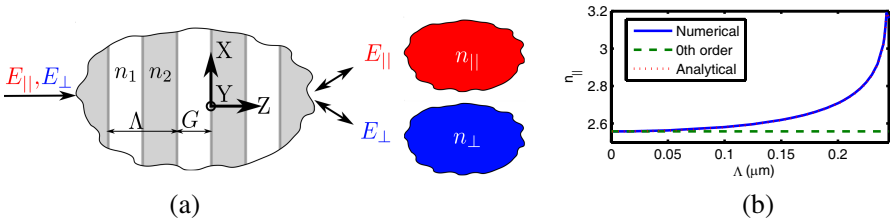

Figure 1. (a) Behaviour of an SWG upon an electrical field parallel ($E_{||}$) and normal ($E_{\perp}$) to the interfaces. (b) Equivalent medium refractive index, $n_{||}$, for $n_1 = 3.476$, $n_2 = 1$ and $G = \Lambda/2$ at $\lambda = 1.55\,\mu$m.

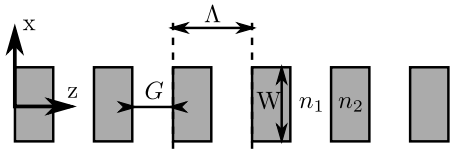

Figure 2. Geometry of a SWG waveguide.

refractive index of the equivalent homogeneous medium depends on the incident field polarization, which can be used to engineer the birefringence [16]. That refractive index can be expressed with the zeroth-order approximation [1]

$$n_{||}^2 = \frac{G}{\Lambda} n_1^2 + \frac{\Lambda - G}{\Lambda} n_2^2 \qquad \frac{1}{n_{\perp}^2} = \frac{G}{\Lambda}\frac{1}{n_1^2} + \frac{\Lambda - G}{\Lambda}\frac{1}{n_2^2} \tag{1}$$

for the electrical field parallel ($n_{||}$) and normal ($n_{\perp}$) to the interfaces. In Figure 1(b), the equivalent refractive index $n_{||}$ of a stratified medium, composed of Silicon ($n \sim 3.5$) and air ($n \sim 1$) layers with a 50% duty cycle, calculated with the numerical tool presented in this paper is compared with the zeroth order approximation [1] and the analytical value [17]. Two conclusions can be extracted. On the one hand, the zeroth-order approximation is only valid for electrically short periods ($2\Lambda n_{\text{eq}}/\lambda \ll 1$). On the other hand, our numerical result and the analytical one are indistinguishable.

While the stratified medium is a convenient structure to understand the SWG principle, many current practical applications use SWG waveguides instead of stratified media [5]. An example of a 2D SWG waveguide is presented in Figure 2, which, in fact, is a stratified medium with a finite width W. In a first order approximation the behaviour of this device is similar to the one of a conventional

waveguide with a homogeneous core [15]. However, SWG parameters, i.e., Λ and G, can be used to engineer the refractive index, the dispersion and the birefringence of the waveguide. If W is not large enough to consider the SWG waveguide as a stratified medium, it cannot be modelled analytically, so that numerical tools are required for its analysis and design.

3. MODELLING OF PERIODIC PHOTONIC DEVICES

In the literature [18, 19], several strategies and methods to analyse photonic devices can be found. They can be classified attending different criteria. In this paper, we have chosen the F-EEM [10, 11], which is a spectral method that belongs to the group of eigenmode expansion methods. It considers structures as longitudinally invariant sections joined by abrupt discontinuities. We have also applied the Floquet modes theory [20, Ch. 9] to the F-EEM. This technique dramatically reduces the computational effort in the analysis of periodic devices [8, 9, 21]. Since SWG structures are typically periodic and exhibit abrupt discontinuities, this method is particularly well suited for their analysis. Below, the F-EEM and the Floquet modes theory are detailed.

3.1. Fourier based Eigenmode Expansion Method

In the F-EEM, we first divide devices into sections in which the refractive index does not depend on the longitudinal coordinate (z). Then, we calculate the eigenmodes of each invariant section as a discrete sum of Fourier coefficients. The complex coordinate Perfectly Matched Layer (PML) boundary conditions are employed to absorb the radiated fields [22]. To propagate the electromagnetic field along the longitudinally invariant sections, we expand the field into the calculated eigenmodes and we use the well-known analytical expressions for mode propagation. The discontinuities are solved using the Mode Matching Method [24, Ch. 9] that matches the tangential fields at both sides of each discontinuity.

So, the first step of the F-EEM is the calculation of the eigenmodes. The simulation tool presented in this paper is based on a 2D version of the F-EEM. In this case, the eigenvalue problem that determines the eigenmodes of each longitudinally invariant section is [10]

$$\overline{\overline{\mathrm{M}}}_i \overline{\overline{\mathrm{T}}}_i = -\overline{\overline{\mathrm{T}}}_i \overline{\overline{\gamma}}_i^2 \tag{2}$$

where the system matrix $\overline{\overline{\mathrm{M}}}_i$ is determined, depending on the light

polarization, by

$$\overline{\overline{\mathrm{M}}}_{TE} = \overline{\overline{\mathrm{P}}}(s_x^{-1})\overline{\overline{\mathrm{D}}}_x\overline{\overline{\mathrm{P}}}(s_x^{-1})\overline{\overline{\mathrm{D}}}_x + k_0^2\overline{\overline{\mathrm{P}}}(\epsilon) \tag{3}$$

for transversal electric (TE) modes and

$$\overline{\overline{\mathrm{M}}}_{TM} = \left[\overline{\overline{\mathrm{P}}}(s_x^{-1})\overline{\overline{\mathrm{D}}}_x\left[\overline{\overline{\mathrm{P}}}(\epsilon)\right]^{-1}\overline{\overline{\mathrm{P}}}(s_x^{-1})\overline{\overline{\mathrm{D}}}_x + k_0^2\overline{\overline{\mathrm{I}}}\right]\left[\overline{\overline{\mathrm{P}}}(\epsilon^{-1})\right]^{-1} \tag{4}$$

for transversal magnetic (TM) modes. The diagonal matrix $\overline{\overline{\gamma}}_i$ is formed by the complex mode propagation constants. The m column of the matrix $\overline{\overline{\mathrm{T}}}_i$ is the Fourier expansion of the m-th mode electrical field. The matrices $\overline{\overline{\mathrm{D}}}_x$ and $\overline{\overline{\mathrm{P}}}()$ are, respectively, the derivative and product operators in the Fourier domain [23]. The matrix $\overline{\overline{\mathrm{I}}}$ is the identity matrix and s_x is a function determined by the PML [22]. The function $\epsilon = \epsilon(x)$ is the relative dielectric function (we omitted x dependence in (3) and (4) for clarity) and $k_0 = 2\pi/\lambda$, where λ is the vacuum wavelength of the electromagnetic field.

Once the eigenvalue problem (2) is solved, the field Fourier coefficients can be calculated as

$$\mathbf{\Phi} = \overline{\overline{\mathrm{T}}}_i\mathbf{\Psi} \tag{5}$$

where $\mathbf{\Psi}$ are the field mode coefficients and $\mathbf{\Phi}$ are the electrical field Fourier coefficients. Then, the propagation of the forward wave $\mathbf{\Psi}^+$ in a longitudinally invariant section is analytically determined by [8]

$$\mathbf{\Psi}^+(z) = \mathrm{e}^{-\overline{\overline{\gamma}}_i(z-z_0)}\mathbf{\Psi}^+(z_0). \tag{6}$$

Note that (6) should not be used to propagate backward modes as the resulting positive exponential can cause numerical problems. To calculate the backward wave, in the tool presented in this paper we have used the reflection coefficient [8]. The reflection coefficient $\overline{\overline{\mathrm{R}}}$ is defined as

$$\mathbf{\Psi}^-(z) = \overline{\overline{\mathrm{R}}}(z)\cdot\mathbf{\Psi}^+(z) \tag{7}$$

and its propagation along a longitudinally invariant section is

$$\overline{\overline{\mathrm{R}}}(z_0) = \mathrm{e}^{-\overline{\overline{\gamma}}(z-z_0)}\cdot\overline{\overline{\mathrm{R}}}(z)\cdot\mathrm{e}^{-\overline{\overline{\gamma}}(z-z_0)} \tag{8}$$

which is attained using negative exponentials that avoid numerical problems. Therefore, once $\mathbf{\Psi}^+$ and $\overline{\overline{\mathrm{R}}}$ are known at the beginning and the end of the longitudinally invariant section respectively, we use Equations (6)–(8) to calculate $\mathbf{\Psi}^\pm$ at any point in that section, solving the propagation problem. Note that the propagation in (6) and (8) is analytical.

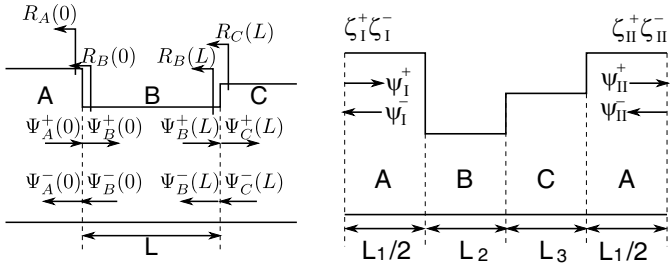

Figure 3. (a) Multiple discontinuity structure. (b) Period sample, letting the period length Λ be $L_1 + L_2 + L_3$.

Finally, let us detail the implementation of the Mode Matching Method used in the presented tool to solve the longitudinal discontinuities [24, Ch. 9]. Consider the interface between two different z-invariant sections A and B where the electrical field is determined by the mode coefficients $\mathbf{\Psi}_A^{\pm}$ and $\mathbf{\Psi}_B^{\pm}$ respectively. According to the continuity condition, we obtain these equations [8]

$$2\mathbf{\Psi}_A^+ = \left(\bar{\bar{\mathrm{e}}}_B + \bar{\bar{\mathrm{h}}}_B\right)\mathbf{\Psi}_B^+ \tag{9}$$

$$\bar{\bar{\mathrm{R}}}_A = \left(\bar{\bar{\mathrm{e}}}_B - \bar{\bar{\mathrm{h}}}_B\right)\left(\bar{\bar{\mathrm{e}}}_B + \bar{\bar{\mathrm{h}}}_B\right)^{-1} \tag{10}$$

where $\bar{\bar{\mathrm{e}}}_B$ and $\bar{\bar{\mathrm{h}}}_B$ are

$$\bar{\bar{\mathrm{e}}}_B = \left(\bar{\bar{\mathrm{T}}}_i^A\right)^{-1}\bar{\bar{\mathrm{T}}}_i^B\left(\bar{\bar{\mathrm{I}}} + \bar{\bar{\mathrm{R}}}_B\right), \quad \bar{\bar{\mathrm{h}}}_B = \left(\bar{\bar{\mathrm{T}}}_i^A\bar{\bar{\mathrm{Y}}}_i^A\right)^{-1}\bar{\bar{\mathrm{T}}}_i^B\bar{\bar{\mathrm{Y}}}_i^B\left(\bar{\bar{\mathrm{I}}} - \bar{\bar{\mathrm{R}}}_B\right) \tag{11}$$

letting $\bar{\bar{\mathrm{Y}}}_i^{A,B}$ be the characteristic admittance matrices [10].

In conclusion, with the expressions (6)–(10), we can analyse waveguide circuits avoiding numerical problems. To do so, consider the structure depicted in Figure 3(a). We first propagate the reflection coefficient $\bar{\bar{\mathrm{R}}}_C(L)$, from the device output to the input using Equations (8) and (10). Then, the forward wave $\mathbf{\Psi}_A^+(0)$, is propagated from the input to the output using (6) and (9). After these two steps, we know $\bar{\bar{\mathrm{R}}}$ and $\mathbf{\Psi}^+$ at any point of the device. Only $\mathbf{\Psi}^-$ remains unknown, but we can calculate it using (7). Note that, using this algorithm, we are able to analyse the whole device without numerical problems and using analytical expressions in the z direction.

3.2. Periodic Devices: The Floquet Modes

The SWG devices that we want to analyse in this paper consist of a periodical sequence of homogeneous sections. Even though the algorithm presented above can be used without numerical problems, we have to perform the mode matching method at least twice per period. As the number of periods may become very high (hundreds or even thousands), the computational effort becomes huge. Floquet modes can be a versatile and useful tool to dramatically reduce the number of operations required to analyse large periodical devices [8].

Floquet modes are the field solution of a periodic structure [20, Ch. 9]. A very intuitive way to calculate the Floquet modes of a periodic device solves an eigenvalue problem based on the transfer matrix relation between the modes at both ends of the period [8]. Although this method works fine when the period length is short, it shows numerical instabilities for long-period devices. This serious drawback can be solved by using the scattering matrix formulation [25], so we have decided to adopt this approach. In our work, we have chosen the latter method so that the presented tool can analyse also long period devices without numerical problems. The actual generalized eigenvalue problem to be solved is

$$\begin{bmatrix} -\overline{\overline{\mathrm{S}}}_{11} & \overline{\overline{\mathrm{I}}} \\ -\overline{\overline{\mathrm{S}}}_{21} & 0 \end{bmatrix} \overline{\overline{\mathrm{X}}} = \begin{bmatrix} 0 & \overline{\overline{\mathrm{S}}}_{12} \\ -\overline{\overline{\mathrm{I}}} & \overline{\overline{\mathrm{S}}}_{22} \end{bmatrix} \overline{\overline{\mathrm{X}}} \begin{bmatrix} \mathrm{e}^{-\overline{\overline{\Gamma}}\Lambda} & 0 \\ 0 & \mathrm{e}^{\overline{\overline{\Gamma}}\Lambda} \end{bmatrix} \tag{12}$$

where Λ is the period length and $\overline{\overline{\mathrm{S}}}$ is the scattering matrix of one period, that is calculated using the algorithm presented in the Section 3.1 and is defined as

$$\begin{bmatrix} \boldsymbol{\Psi}_I^- \\ \boldsymbol{\Psi}_{II}^+ \end{bmatrix} = \begin{bmatrix} \overline{\overline{\mathrm{S}}}_{11} & \overline{\overline{\mathrm{S}}}_{12} \\ \overline{\overline{\mathrm{S}}}_{21} & \overline{\overline{\mathrm{S}}}_{22} \end{bmatrix} \begin{bmatrix} \boldsymbol{\Psi}_I^+ \\ \boldsymbol{\Psi}_{II}^- \end{bmatrix} \tag{13}$$

where $\boldsymbol{\Psi}_{I,II}^{\pm}$ are the mode coefficients at the left (I) and right (II) end of the period, represented in Figure 3(b). The eigenvalues of (12) are the elements of the diagonal matrix $\mathrm{e}^{-\overline{\overline{\Gamma}}\Lambda}$, where $\overline{\overline{\Gamma}}$ is a diagonal matrix whose elements represent the complex propagation constant of the Floquet modes. The eigenvectors are the Floquet modes waveguide coefficients, arranged in the columns of $\overline{\overline{\mathrm{X}}}$, letting the relation between the Floquet modes and the waveguide modes be

$$\begin{bmatrix} \boldsymbol{\Psi}_q^+ \\ \boldsymbol{\Psi}_q^- \end{bmatrix} = \overline{\overline{\mathrm{X}}} \cdot \begin{bmatrix} \zeta_q^+ \\ \zeta_q^- \end{bmatrix} = \begin{bmatrix} \overline{\overline{\mathrm{X}}}_1 & \overline{\overline{\mathrm{X}}}_2 \\ \overline{\overline{\mathrm{X}}}_3 & \overline{\overline{\mathrm{X}}}_4 \end{bmatrix} \cdot \begin{bmatrix} \zeta_q^+ \\ \zeta_q^- \end{bmatrix} \tag{14}$$

were $\zeta_q^{\pm}$ and $\boldsymbol{\Psi}_q^{\pm}$ are, respectively, the Floquet and waveguide mode coefficients at the beginning of the period q, as depicted in Figure 3(b).

Besides, propagation of forward Floquet modes ζ^+ between the left ends of periods q and r is

$$\zeta_r^+ = \mathrm{e}^{-\overline{\overline{\Gamma}}\Lambda(r-q)}\zeta_q^+. \tag{15}$$

Again, numerical problems arise if (15) is used in the propagation of backward Floquet modes ζ^-. The Floquet mode reflection coefficient is used to avoid numerical problems [8]. The Floquet reflection coefficient $\overline{\overline{\xi}}$ is defined by

$$\zeta_q^- = \overline{\overline{\xi}}_q \zeta_q^+ \tag{16}$$

and its propagation is expressed as [8]

$$\overline{\overline{\xi}}_q = \mathrm{e}^{-\Gamma\Lambda(r-q)}\overline{\overline{\xi}}_r \mathrm{e}^{-\Gamma\Lambda(r-q)}. \tag{17}$$

From (7), (14) and (16), the relation between waveguide and Floquet reflection coefficients is

$$\overline{\overline{\mathrm{R}}} = \left(\overline{\overline{\mathrm{X}}}_3 + \overline{\overline{\mathrm{X}}}_4\overline{\overline{\xi}}\right)\left(\overline{\overline{\mathrm{X}}}_2\overline{\overline{\xi}} + \overline{\overline{\mathrm{X}}}_1\right)^{-1}, \quad \overline{\overline{\xi}} = \left(\overline{\overline{\mathrm{R}}}\,\overline{\overline{\mathrm{X}}}_2 - \overline{\overline{\mathrm{X}}}_4\right)^{-1}\left(\overline{\overline{\mathrm{X}}}_3 - \overline{\overline{\mathrm{R}}}\,\overline{\overline{\mathrm{X}}}_1\right). \tag{18}$$

Finally, we describe the algorithm to analyse the whole device. First, the waveguide reflection coefficient at the structure output is transformed into Floquet mode reflection coefficient using (18). We transform the output Floquet reflection coefficient to the input with (17). Using (18), we get the waveguide reflection coefficient at the input. It allows us to calculate the field distribution at the input once the incident field is known. Then, using (14)–(16), we can determine the field distribution in the whole device. Note that numerical problems are not expected as positive exponentials have been avoided and the S-matrix formulation has been used.

In conclusion, we have detailed two techniques to analyse photonic devices. On the one hand, the F-EEM is used on a generic structure and is specially efficient with structures formed by longitudinally invariant structures joined by abrupt discontinuities. On the other hand, the Floquet modes efficiently analyse long periodic devices, giving a better physical insight of the device performance.

4. FEXEN

In this section, we present the Fourier EXpansion simulation ENvironment (FEXEN), which is the simulation tool that we present in this paper. The electromagnetic core of this tool implements the F-EEM with Floquet modes theory, already detailed in the previous section. Besides, it includes a set of functionalities aimed to ease the design of photonic devices and, particularly of SWG structures.

The overall result is a set of MATLAB functions implementing a 2D CAD tool that, up to now, has been successfully used in the analysis and design of several photonic devices [12, 14, 26]. It is worth mentioning that the reliability of FEXEN was demonstrated elsewhere [13, Figure 3], where the results of this tool were fairly similar to actual measurements on a real device. To understand the set of functionalities offered by FEXEN, we will classify them in three different groups: i) electromagnetic simulation features, ii) automation characteristics and iii) simulator output options.

The main electromagnetic simulation characteristics of FEXEN are the same of any other CAD tool based on the eigenmode expansion method. On the one hand, modal analysis of longitudinally invariant structures can be calculated. On the other hand, the electromagnetic field propagation is simulated. Besides, when periodic structures are involved, Floquet modes can be obtained. FEXEN can also handle circuital ports that, combined with the previous features, let the designer efficiently calculate the scattering parameters of multi-port periodic devices. As a final detail, the tool offers some smart options to customize the input field and the load condition, such as a weighted sum of port modes or a Gaussian distribution for the input field, and a perfect mirror or a semi-infinite periodic structure for the load condition.

Automation features let the designer evaluate many different design options with a single instruction. We have provided FEXEN with a sweep system that allows the simultaneous variation of all the variables the user may define. This feature was essential for the design of the MMI coupler with 2D SWG cladding that will be presented in Section 5.3. The designer can also automate the structure definition. To do so, this tool allows the user to divide the whole device in zones. Then, several zone types are provided and each of them allows the smart definition of different structures. In the Figure 4, we present three different structures automatically generated by FEXEN: a) a periodic structure, b) a longitudinally variant structure, and c) a combination of both of them.

Finally, let us focus on the simulator output. It is determined by customized simulation scripts that define the analysis to be performed on the photonic structure. Therefore, depending on the executed script, different results can be obtained. The use of scripts provides FEXEN with a representation versatility just limited by MATLAB capabilities and the designer ability. The tool includes predefined scripts to calculate usual characteristics, such us Floquet mode effective indices, scattering parameters, electromagnetic field propagation or power flux along arbitrarily defined segments. Note that more

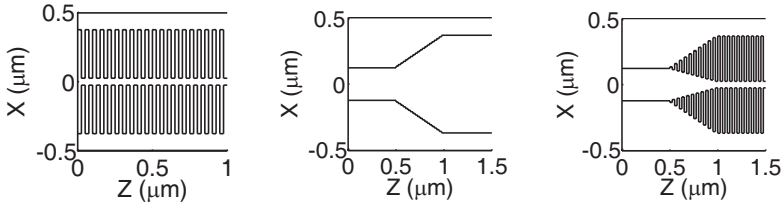

Figure 4. Three different automatically generated structures: (a) Grating, (b) taper and (c) SWG taper.

complicated figures of merit can be obtained. For example, the phase error and the common mode rejection ratio in a 90° hybrid [14] or the coupling efficiency between a radiating grating and a fibre [12] were obtained using customized FEXEN scripts.

5. RESULTS

In this work, we have used the presented tool to analyse three different structures comprising SWG. The first one is a directional coupler with two SWG waveguides. We have analysed this simple device to show the SWG behaviour and to validate the presented tool. The second analysed device is a recently designed 90° hybrid receiver implemented by a multi-modal interference (MMI) device that includes an SWG cladding to engineer the index contrast and achieve a better performance [14]. We use this device to show the capability of FEXEN to aid the design of novel devices comprising SWG structures. Finally, the third device is an improvement of the previous one. It will be shown for the first time that using a rather involved 2D SWG cladding, the fabrication tolerances can be doubled, compared to the previously reported design [14]. The use of an efficient design tool is indispensable in this problem, since the number of geometrical parameters to be designed is significantly greater in this case.

5.1. Directional Coupler with two SWG Parallel Waveguides

The conventional directional coupler is a well-known device that has been analysed widely in the literature, e.g., [27, Ch. 3]. It consist of two parallel waveguides separated a distance W_g, as depicted in Figure 5(a). When light is injected in one of the waveguides, at the coupling length L_π, light has coupled to the other waveguide. The coupling length is

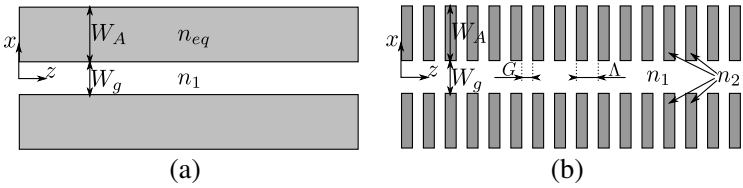

Figure 5. Directional couplers: (a) with homogeneous waveguides, and (b) with SWG waveguides.

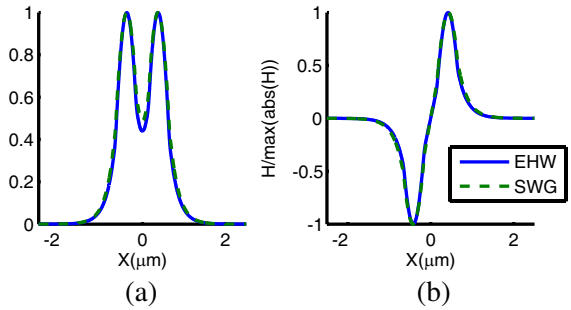

Figure 6. (a) Even and (b) odd supermodes of a directional coupler formed by SWG (dashed line) [Figure 5(b))] or the conventional coupler with EHW (solid line) [Figure 4(a))].

a function of the structure refractive indices, the waveguides geometry and the separation between them.

In this paper, we substitute the waveguides with homogeneous core of a conventional directional coupler by SWG waveguides, as shown in Figure 5(b). Thanks to that, the effective index and the chromatic dispersion of the constituent waveguides can be engineered. This could lead to novel applications such us filters. In Figure 6, we represent the supermodes of the conventional and SWG couplers. The dashed lines represent the even and odd TM supermodes of the SWG directional coupler letting $W_A = 0.5\,\mu\text{m}$, $W_g = 0.3\,\mu\text{m}$, $\Lambda = 0.1\,\mu\text{m}$ and $G = 50\,\text{nm}$. The free-space wavelength is $\lambda = 1.55\,\mu\text{m}$, the core refractive index is $n_2 = 2.85$ and the cladding is $n_1 = 1.58$. In these conditions, the SWG waveguides are equivalent to homogeneous waveguides of the same width W_A and a core refractive index $n_{eq} = 2.25$, that we calculated using our tool. The solid line in Figure 6 represent, at $\lambda = 1.55\,\mu\text{m}$, the TM supermodes of the directional coupler formed by the equivalent homogeneous waveguides (EHW) with $n_{eq} = 2.25$ [Figure 5(a)]. Both supermodes are in a very good agreement.

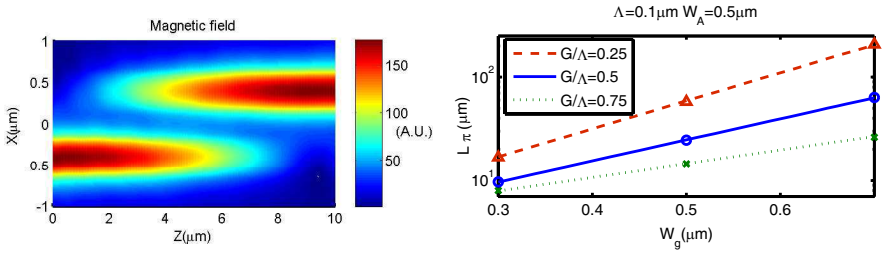

Figure 7. (a) Field propagation in a SWG coupler. (b) Coupling length versus waveguide separation in a SWG directional coupler. Curves calculated with FEXEN while markers calculated with an FDTD commercial tool.

We have used FEXEN to predict the SWG coupler coupling length against waveguide separation [Figure 5(b)]. The field propagation is presented in the Figure 7(a), where the power transfer between both waveguides can be appreciated. The coupling length (L_π) can be expressed as $L_\pi = \pi/(\beta_1 - \beta_2)$, where β_1 and β_2 are the propagation constants of the even and odd supermodes respectively. Note that these supermodes are Floquet modes. Programming an appropriate script, the coupling length against waveguide separation, shown in Figure 7(b), was automatically plotted by our tool. To confirm these results, we simulated the same coupler on a commercial 2D FDTD tool (RSoft FullWAVE). FDTD results are marked on the same figure. As can be seen, both results are in a very good agreement (maximum error is 2.8%). It is worth mentioning that each FEXEN simulation point was calculated in less than 10 seconds using an 8 core @ 2.8 GHz with 8 GB RAM PC while each FDTD point took from 10 minutes in the shortest simulation to 24 hours in the longest one. These numbers show that EEM is better suited than FDTD for analysis and design of SWG structures.

5.2. High Performance MMI Using SWG

An MMI is a well known structure widely used in photonic circuits, such us Mach-Zehnder interferometers [28] or 90° hybrid for coherent optical receivers [29]. As shown in [29], MMI performance can be highly improved optimizing the index contrast. While this solution required two etch steps, the use of SWG can reduce the index contrast employing only one etch step, which reduces the fabrication complexity. Based on that concept, FEXEN was used to design the novel SWG based 2×4 MMI shown in Figure 8(a) [14].

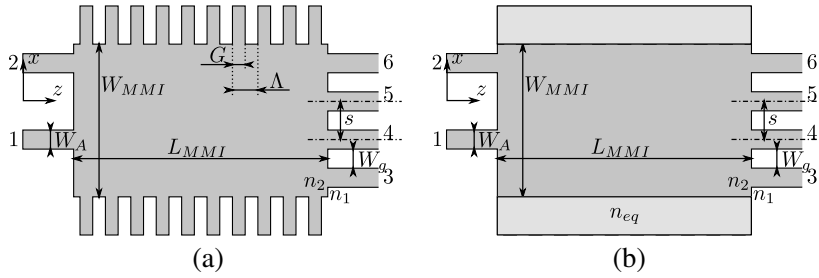

Figure 8. High performance MMI for coherent optical reception using: (a) SWG structure cladding and (b) Homogeneous cladding.

The design process of this device, detailed by Ortega et al. [14], is summarized as follows. First we design an MMI with homogeneous cladding, as the one depicted in Figure 8(b). Then, we calculate the SWG structure that synthesizes the homogeneous cladding. Finally, we adjust the resulting device [Figure 8(a)].

The first step does not involve any SWG structure, so we will just indicate the results. Considering the working wavelength $\lambda = 1.55\,\mu\text{m}$ the homogeneous MMI parameters are $W_A = 1.5\,\mu\text{m}$, $W_g = 0.5\,\mu\text{m}$, $W_{MMI} = 7.7\,\mu\text{m}$, $L_{MMI} = 116\,\mu\text{m}$ and $n_{eq} = 2.62$. The refractive indices are $n_1 = 1.58$ and $n_2 = 2.85$, which have been calculated using the effective index method on a SOI waveguide formed by a SiO_2 bottom oxide ($n_{SiO_2} = 1.444$), a 260 nm thick Si core ($n_{Si} = 3.476$) and a SU-8 cladding ($n_{SU\text{-}8} = 1.58$).

In the second step, we design a SWG structure that synthesize a refractive index $n_{eq} = 2.62$. To do so, we first use FEXEN Floquet mode calculation to obtain a set of curves that relate n_{eq} with the gap (G) and pitch (Λ) of a stratified medium. These curves are presented in the Figure 9(a). Depending on the gap size chosen, we get different optimum pitches. Then, we select a pair (Λ, G) that implements the desired n_{eq}. In this case, we elected $G = 80\,\text{nm}$ which leads to a pitch $\Lambda \approx 270\,\text{nm}$.

Finally, we finely adjust the resulting device. This adjustment is needed because the actual device is different from the problem considered in the previous step: the SWG is not infinitely wide and the fundamental mode in the SWG is not a plane wave. In Figure 9(b), we have represented the modal phase error, as defined elsewhere [29], for three different pitches. To obtain high performance MMI, the modal phase error should be as low as possible. We found out that the optimum pitch is slightly shorter than initially predicted. Again, a CAD tool supporting Floquet modes, such as FEXEN, can efficiently calculate these curves.

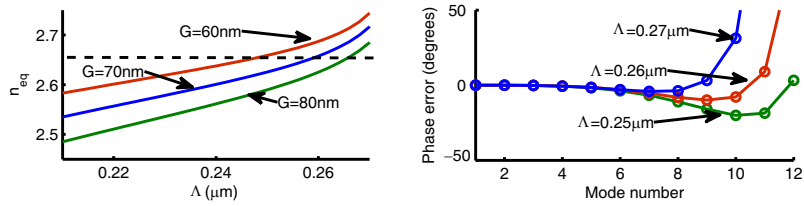

Figure 9. Figures to aid the design of the SWG part. (a) Equivalent refractive index of a stratified medium versus its pitch and gap sizes. (b) Modal phase error of an SWG MMI: $W_{MMI} = 7.7\,\mu\text{m}$, $G = 80\,\text{nm}$, $n_1 = 1.58$, $n_2 = 2.85$, and $\lambda = 1.55\,\mu\text{m}$.

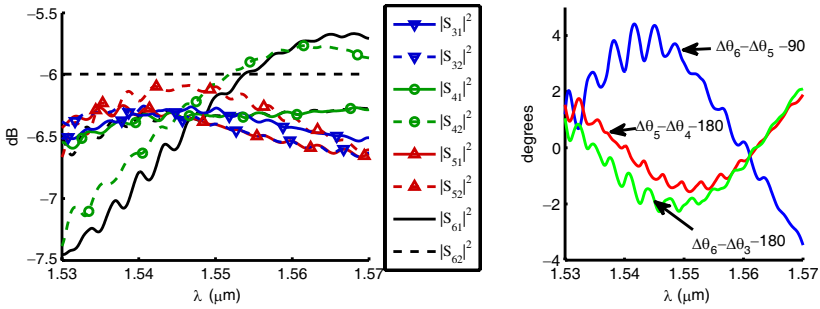

Figure 10. SWG MMI behaviour in (a) amplitude and (b) phase, where $\Delta\theta_i = \angle(S_{i1}/S_{i2})$.

Choosing $\Lambda = 260\,\text{nm}$ and an MMI length of 446 periods we use the FEXEN functionality to calculate the scattering parameters of a multi-port periodic device. The device features are shown in Figure 10. On the one hand, Figure 10(a) shows the amplitude behaviour of the device. The optimum value is $-6\,\text{dB}$, as the power is divided among four ports. The resulting power imbalance is lower than 0.5 dB in the central wavelength and the maximum insertion loss is lower than 1.5 dB in the C band (1530–1570 nm). On the other hand, we can see in the Figure 10(b) that the device phase error is very good (lower than 5° in the whole C-band).

5.3. MMI with 2D SWG Structure

Even though the device presented above theoretically performs properly, the actual fabricated circuit may differ from the nominal

design. The tolerance analysis of it concludes that gap (G) deviations larger than 5 nm make the device not satisfy the coherent photonic receiver specifications [30] in the C-band bandwidth. To improve the tolerance to fabrication errors, we propose the new device presented in Figure 11. It presents a larger critical dimension than the previous structure, reducing the dependence of the device behaviour with fabrication errors.

The design procedure is similar to the one specified for the previous device, but there are some differences as new degrees of freedom appear (G_X, Λ_X) as shown in Figure 11(b). We have first chosen $\Lambda_Z = 240$ nm as it is close to the largest pitch that allows SWG behaviour. We have also forced $G_Z = G_X$, i.e., squared holes, as they minimize effective index deviation with fabrication errors. Then, we have programmed a script to calculate the bandwidth where the mentioned specifications are satisfied and we automatically evaluated it in reasonable combinations of $G_X = G_Z$ and Λ_X. The results are shown in Figure 12 where appropriate devices are represented by light colours. Note that these figures summarize the S parameters calculation of more than one hundred different devices at 21 different wavelengths. The total computation time in the equipment previously mentioned was shorter than 24 hours, which is a very reasonable time. According to these figures, we chose the following design parameters: $\Lambda_Z = 240$ nm, $G_Z = G_X = 130$ nm and $\Lambda_X = 420$ nm. Using them, we obtained the behaviour shown in Figure 13, where it can be seen that fabrication errors of 10 nm do not reduce the bandwidth below 40 nm, i.e., the C-band bandwidth. So, using the advanced automation capabilities of the presented tool, we have been able to design a device, with two more degrees of freedom, that duplicates the fabrication tolerance of the previous one.

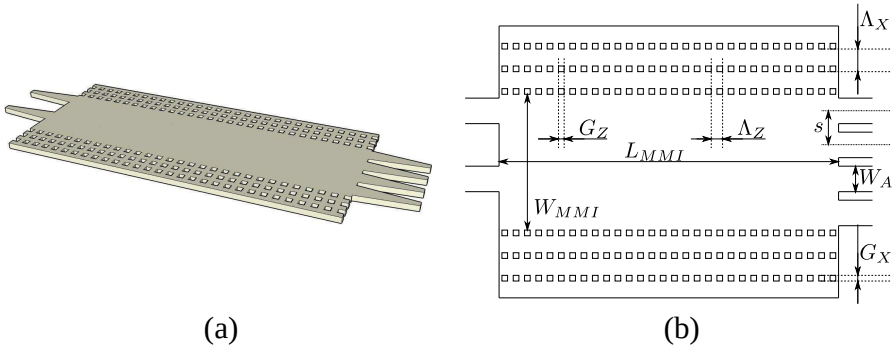

Figure 11. Representation of a 2D SWG MMI. (a) 3D view and (b) top view with parameters identification.

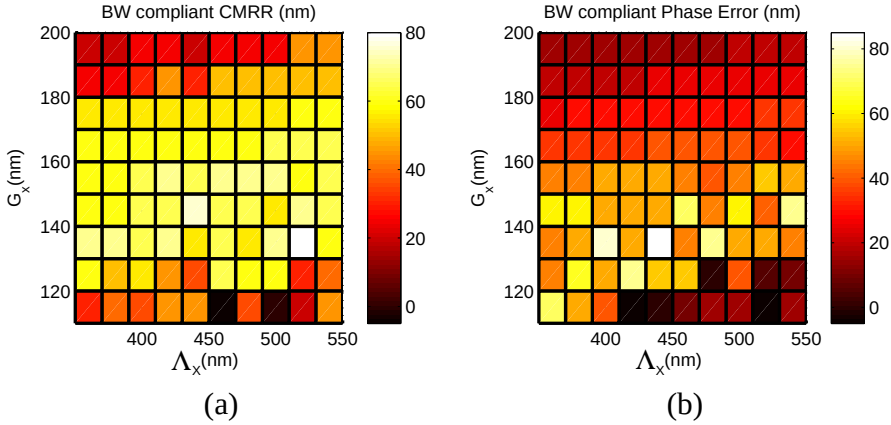

Figure 12. Bandwidth (BW) in which the device satisfies (a) CMRR and (b) Phase error coherent receiver specifications [30].

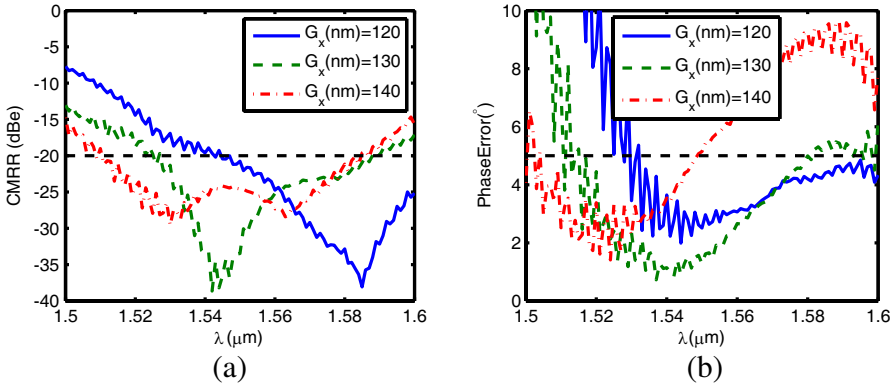

Figure 13. Device performance: (a) CMRR and (b) phase error.

6. CONCLUSION

We have presented a tool to aid the design of periodical structures, such as SWG structures. It is based on the Fourier Eigenmode Expansion Method and includes the Floquet modes theory to efficiently analyse periodic structures. Besides, the most interesting implemented functionalities to ease the design of photonic devices have been detailed. We have finally shown the tool capabilities using it to analyse and design three different devices with SWG structures. We have also shown that the proposed method is better suited to analyse and design SWG structures than FDTD, typically used in the literature.

ACKNOWLEDGMENT

This work was supported in part by the Spanish Ministerio de Ciencia (project TEC2009-10152), a Formación del Profesorado Universitario scholarship (AP-2006-03355), and by the Andalusian Regional Ministry of Science (project TIC-02946).

REFERENCES

1. Rytov, S. M., "Electromagnetic properties of a finely stratified medium," *Sov. Phys. JETP*, Vol. 2, No. 3, 466–475, 1956.
2. Lalanne, P. and J.-P. Hugonin, "High-order effective-medium theory of subwavelength gratings in classical mounting: Application to volume holograms," *J. Opt. Soc. Am. A*, Vol. 15, No. 7, 1843–1851, Jul. 1998.
3. Mateus, C., M. Huang, L. Chen, C. Chang-Hasnain, and Y. Suzuki, "Broad-band mirror (1.12–1.62 µm) using a subwavelength grating," *IEEE Photonics Technology Letters*, Vol. 16, No. 7, 1676–1678, Jul. 2004.
4. Halir, R., P. Cheben, S. Janz, D.-X. Xu, I. Molina-Fernández, and J. G. Wangüemert-Pérez, "Waveguide grating coupler with subwavelength microstructures," *Opt. Lett.*, Vol. 34, No. 9, 1408–1410, 2009.
5. Bock, P. J., P. Cheben, J. H. Schmid, J. Lapointe, A. Delâge, D.-X. Xu, S. Janz, A. Densmore, and T. J. Hall, "Subwavelength grating crossings for silicon wire waveguides," *Opt. Express*, Vol. 18, No. 15, 16146–16155, 2010.
6. Butt, H., Q. Dai, T. D. Wilkinson, and G. A. J. Amaratunga, "Photonic crystals & metamaterial filters based on 2D arrays of silicon nanopillars," *Progress In Electromagnetic Research*, Vol. 113, 179–194, 2011.
7. Shi, Y., "A compact polarization beam splitter based on a multimode photonic crystal waveguide with an internal photonic crystal section," *Progress In Electromagnetic Research*, Vol. 103, 393–401, 2010.
8. Helfert, S. F. and R. Pregla, "The method of lines: A versatile tool for the analysis of waveguide structures," *Electromagnetics*, Vol. 22, No. 8, 615–637, 2002.
9. Čtyroký, J., S. Helfert, and R. Pregla, "Analysis of a deep waveguide Bragg grating," *Optical and Quantum Electronics*, Vol. 30, 343–358, 1998.

10. Ortega-Moñux, A., I. Molina-Fernández, and J. G. Wangüemert-Pérez, "3D-scalar Fourier eigenvector expansion method (Fourier-EEM) for analyzing optical waveguide discontinuities," *Optical and Quantum Electronics*, Vol. 37, No. 1, 213–228, 2005.
11. Hugonin, J. P., P. Lalanne, I. D. Villar, and I. R. Matias, "Fourier modal methods for modeling optical dielectric waveguides," *Optical and Quantum Electronics*, Vol. 37, 107–119, 2005.
12. Alonso-Ramos, C., A. Ortega-Moñux, I. Molina-Fernández, P. Cheben, L. Zavargo-Peche, and R. Halir, "Efficient fiber-to-chip grating coupler for micrometric SOI rib waveguides," *Opt. Express*, Vol. 18, No. 14, 15189–15200, Jul. 2010.
13. Alonso-Ramos, C., A. Ortega-Moñux, L. Zavargo-Peche, R. Halir, J. de Oliva-Rubio, I. Molina-Fernãndez, P. Cheben, D.-X. Xu, S. Janz, N. Kim, and B. Lamontagne, "Single-etch grating coupler for micrometric silicon rib waveguides," *Opt. Lett.*, Vol. 36, No. 14, 2647–2649, 2011.
14. Ortega-Moñux, A., L. Zavargo-Peche, A. Maese-Novo, I. Molina-Fernández, R. Halir, J. G. Wangüemert-Pérez, P. Cheben, and J. H. Schmid, "High performance multimode interference coupler in silicon waveguides with subwavelength structures," *IEEE Photonics Technology Letters*, Vol. 23, No. 19, 1406–1135, 2011.
15. Cheben, P., P. J. Bock, J. H. Schmid, J. Lapointe, S. Janz, D.-X. Xu, A. Densmore, A. Delâge, B. Lamontagne, and T. J. Hall, "Refractive index engineering with subwavelength gratings for efficient microphotonic couplers and planar waveguide multiplexers," *Opt. Lett.*, Vol. 35, No. 15, 2526–2528, 2010.
16. Chen, D., M.-L. Vincent Tse, and H.-Y. Tam, "Optical properties of photonic crystal fibers with a fiber core of arrays of subwavelength circular air holes: Birefringence and dispersion," *Progress In Electromagnetic Research*, Vol. 105, 193–212, 2010.
17. Yariv, A. and P. Yeh, "Electromagnetic propagation in periodic stratified media. ii. Birefringence, phase matching, and x-ray lasers," *J. Opt. Soc. Am.*, Vol. 67, No. 4, 438–448, 1977.
18. Scarmozzino, R., A. Gopinath, R. Pregla, and S. Helfert, "Numerical techniques for modeling guided-wave photonic devices," *IEEE Journal of Selected Topics in Quantum Electronics*, Vol. 6, No. 1, 150–162, 2000.
19. Besbes, M., J. Hugonin, P. Lalanne, S. van Haver, O. Janssen, A. Nugrowati, M. Xu, S. Pereira, H. Urbach, A. van de Nes, P. Bienstman, G. Granet, A. Moreau, S. Helfert, M. Sukharev, T. Seideman, F. Baida, B. Guizal, and D. van Labeke, "Numerical analysis of a slit-groove diffraction problem," *J. Europ. Opt. Soc.*

Rap. Public., Vol. 2, No. 07022, 1–17, 2007.

20. Collin, R. E., *Field Theory of Guided Waves*, 2nd edition, IEEE Press, New York, 1991.
21. Watanabe, K. and K. Yasumoto, "Accuracy improvement of the Fourier series expansion method for Floquet-mode analysis of photonic crystal waveguides," *Progress In Electromagnetics Research*, Vol. 92, 209–222, 2009.
22. Wangümert-Pérez, J., I. Molina-Fernández, and M. Luque-Nieto, "A novel Fourier based 3D full-vectorial beam propagation method," *Optical and Quantum Electronics*, Vol. 36, 285–301, 2004.
23. Molina-Fernández, I. and J. Wangüemert-Pérez, "Variable transformed series expansion approach for the analysis of nonlinear guided waves in planar dielectric waveguides," *Journal of Lightwave Technology*, Vol. 16, No. 7, 1354–1363, Jul. 1998.
24. Itoh, T., *Numerical Techniques for Microwave and Millimeter-Wave Passive Structures*, Wiley, 1989.
25. Cao, Q., P. Lalanne, and J.-P. Hugonin, "Stable and efficient Bloch-mode computational method for one-dimensional grating waveguides," *J. Opt. Soc. Am. A*, Vol. 19, No. 2, 335–338, 2002.
26. Scott, A., P. Bock, C. A. Alonso-Ramos, B. Lamontagne, P. Cheben, M. Florjanczyk, I. Molina-Fernández, S. Janz, A. Ortega-Monux, B. Solheim, and D.-X. Xu, "Improved coupling to integrated spatial heterodyne spectrometers with applications to space," *SPIE*, S. Garcia-Blanco and R. Ramesham (eds.), Vol. 7928, No. 1, 79280K, 2011.
27. Tamir, T., *Guided-wave Optoelectronics*, ser. Springer Series in Electronics and Photonics, Springer-Verlag, 1988.
28. Kim, D. W., A. Barkai, R. Jones, N. Elek, H. Nguyen, and A. Liu, "Silicon-on-insulator eight-channel optical multiplexer based on a cascade of asymmetric Mach-Zehnder interferometers," *Opt. Lett.*, Vol. 33, No. 5, 530–532, Mar. 2008.
29. Halir, R., G. Roelkens, A. Ortega-Moñux, and J. G. Wangüemert-Pérez, "High-performance 90° hybrid based on a silicon-on-insulator multimode interference coupler," *Opt. Lett.*, Vol. 36, No. 2, 178–180, 2011.
30. Implementation agreement for integrated dual polarization intradyne coherent receivers, Optical Internetworking Forum, 2010. Available: http://www.oiforum.com/public/documents/OIF_DP-C_RX-01.0.pdf.